



RESEARCH ARTICLE

# Wharton's Jelly mesenchymal stromal cell-derived extracellular vesicles promote nucleus pulposus cell anabolism in an in vitro 3D alginate-bead culture model

Veronica Tilotta<sup>1</sup> | Gianluca Vadalà<sup>1,2</sup>  | Luca Ambrosio<sup>1,2</sup>  |  
Giuseppina Di Giacomo<sup>1</sup> | Claudia Cicione<sup>1</sup> | Fabrizio Russo<sup>1,2</sup> |  
Adas Darinskas<sup>3,4</sup> | Rocco Papalia<sup>1,2</sup> | Vincenzo Denaro<sup>2</sup>

<sup>1</sup>Laboratory for Regenerative Orthopaedics, Research Unit of Orthopaedic and Trauma Surgery, Department of Medicine and Surgery, Università Campus Bio-Medico di Roma, Rome, Italy

<sup>2</sup>Operative Research Unit of Orthopaedic and Trauma Surgery, Fondazione Policlinico Universitario Campus Bio-Medico, Rome, Italy

<sup>3</sup>Laboratory of Immunology, National Cancer Institute, Vilnius, Lithuania

<sup>4</sup>JSC Innovita Research, Tissue Bank, Vilnius, Lithuania

## Correspondence

Gianluca Vadalà, Department of Orthopaedic and Trauma Surgery, Campus Bio-Medico University Hospital Foundation, Via Alvaro del Portillo 200, 00128, Rome, Italy.  
Email: [g.vadala@policlinicocampus.it](mailto:g.vadala@policlinicocampus.it)

## Funding information

Horizon 2020 Framework Programme, Grant/Award Number: 732163

## Abstract

**Background:** Intradiscal transplantation of mesenchymal stromal cells (MSCs) has emerged as a promising therapy for intervertebral disc degeneration (IDD). However, the hostile microenvironment of the intervertebral disc (IVD) may compromise the survival of implanted cells. Interestingly, studies reported that paracrine factors, such as extracellular vesicles (EVs) released by MSCs, may regenerate the IVD. The aim of this study was to investigate the therapeutic effects of Wharton's Jelly MSC (WJ-MSC)-derived EVs on human nucleus pulposus cells (hNPCs) using an in vitro 3D alginate-bead culture model.

**Methods:** After EV isolation and characterization, hNPCs isolated from surgical specimens were encapsulated in alginate beads and treated with 10, 50, and 100 µg/mL WJ-MSC-EVs. Cell proliferation and viability were assessed by flow cytometry and live/dead staining. Nitrite and glycosaminoglycan (GAG) content was evaluated through Griess and 1,9-dimethylmethylene blue assays. hNPCs in alginate beads were paraffin-embedded and stained for histological analysis (hematoxylin-eosin and Alcian blue) to assess extracellular matrix (ECM) composition. Gene expression levels of catabolic (*MMP1*, *MMP13*, *ADAMT5*, *IL6*, *NOS2*), anabolic (*ACAN*), and hNPC marker (*SOX9*, *KRT19*) genes were analyzed through qPCR. Collagen type I and type II content was assessed with Western blot analysis.

**Results:** Treatment with WJ-MSC-EVs resulted in an increase in cell content and a decrease in cell death in degenerated hNPCs. Nitrite production was drastically reduced by EV treatment compared to the control. Furthermore, proteoglycan content was enhanced and confirmed by Alcian blue histological staining. EV stimulation attenuated ECM degradation and inflammation by suppressing catabolic and inflammatory gene expression levels. Additionally, NPC phenotypic marker genes were also maintained by the EV treatment.

**Conclusions:** WJ-MSC-derived EVs ameliorated hNPC growth and viability, and attenuated ECM degradation and oxidative stress, offering new opportunities for

This is an open access article under the terms of the [Creative Commons Attribution-NonCommercial-NoDerivs](https://creativecommons.org/licenses/by-nc-nd/4.0/) License, which permits use and distribution in any medium, provided the original work is properly cited, the use is non-commercial and no modifications or adaptations are made.

© 2023 The Authors. *JOR Spine* published by Wiley Periodicals LLC on behalf of Orthopaedic Research Society.

IVD regeneration as an attractive alternative strategy to cell therapy, which may be jeopardized by the harsh microenvironment of the IVD.

#### KEYWORDS

exosome, extracellular vesicles, intervertebral disc, intervertebral disc degeneration, intervertebral disc regeneration, low back pain, mesenchymal stromal cells

## 1 | INTRODUCTION

Low back pain (LBP) has a significant impact on the society, affecting more than 85% of the global population and representing the leading cause of disability worldwide.<sup>1</sup> The main cause of LBP is related to intervertebral disc degeneration (IDD), whose pathophysiology remains poorly understood. Multiple factors seem to be involved in the process, including mechanical overload, aging, metabolic disorders, trauma, insufficient nutrient supply, smoking, and genetic predisposition.<sup>2-4</sup> However, the underlying mechanisms have not yet been fully identified.<sup>5</sup>

The intervertebral disc (IVD) is the largest avascular organ of the human body and is composed of three tissues: the annulus fibrosus (AF), which surrounds the nucleus pulposus (NP), and the cartilaginous endplates (CEPs) at both upper and lower vertebral surfaces. The NP has a gel-like structure rich in proteoglycans that attract water to maintain its shock-absorbing ability. IDD is characterized by increased NP cell death and senescence, with consequent degradation of the extracellular matrix (ECM), NP dehydration, and progressive loss of disc height, with nerve ingrowth, CEP calcification, accumulation of inflammatory cytokines including interleukin (IL)-1 $\beta$ , and structural deterioration.<sup>6</sup>

Presently, treatment approaches for LBP are mainly symptomatic and unable to tackle the degenerative process.<sup>7</sup> In the last decades, intradiscal transplantation of mesenchymal stromal cells (MSCs) has proven to be a promising tool for treating IDD both in preclinical and clinical trials.<sup>8-10</sup> Indeed, MSCs have been shown to promote nucleus pulposus cell (NPCs) proliferation with enhanced production of ECM and reduction of apoptosis, differentiate into NPCs, and modulate immune responses.<sup>11</sup> However, MSC survival is significantly challenged by the hostile microenvironment within the degenerative IVD, which may importantly limit the efficacy of intradiscal cell therapy.<sup>12</sup> Recently, growing evidence has suggested that MSCs mainly exert their therapeutic effects through the secretion of bioactive molecules and paracrine mediators, such as extracellular vesicles (EVs).<sup>13</sup> EVs have been reported to be involved in cell-to-cell communication by delivering proteins, lipids, mRNA, miRNA, noncoding RNA, and ribosomal RNA.<sup>14</sup> Emerging results suggest that EVs play a crucial role in numerous physiological processes by regulating the fate of recipient cells, and are being increasingly investigated as biomarkers or drug delivery carriers.<sup>15</sup> However, the mechanisms behind EV effects are not fully understood and thus need further investigation.

In the last decade, MSC-derived EVs have been shown to exert potent anabolic effects on IVD cells, including reduced NPC

apoptosis, lower ECM degradation, decreased levels of oxidative stress and inflammatory mediators, and enhanced chondrogenic NPC differentiation and proliferation, both in vitro and in vivo.<sup>16</sup> Among the MSC types investigated, little evidence has been described concerning Wharton's Jelly MSCs (WJ-MSCs). WJ-MSCs reside in the umbilical cord and, like adult MSCs, express typical MSC surface markers, exhibit plastic adherence, and are able to differentiate toward osteogenic, chondrogenic, and adipogenic lineages.<sup>17</sup> Remarkably, WJ-MSCs represent a young MSC source with a high proliferation rate, phenotype retention over multiple in vitro passages, lower immunogenicity and tumorigenicity, and greater ex vivo expansion capabilities compared to bone marrow (BM)-derived MSCs.<sup>18</sup> Furthermore, WJ-MSCs have been previously shown to differentiate towards an NPC phenotype, protect NPCs from apoptosis, and induce ECM production with increased disc height and IVD hydration in vivo.<sup>19</sup> Interestingly, EVs harvested by this MSC subpopulation have yielded promising results in several other preclinical models of inflammatory and degenerative disorders (e.g., Parkinson's disease, osteoarthritis, etc.),<sup>20,21</sup> although no previous study has specifically investigated their potential regenerative effects on IDD.

The aim of this study was to evaluate the effect of EVs derived from Wharton's Jelly MSCs (WJ-MSC-EVs) on human NP cells (hNPCs) using a 3D alginate-bead culture model in vitro. We hypothesized that WJ-MSC-EVs might enhance hNPC proliferation, viability, ECM production, and limit their inflammatory state.

## 2 | MATERIALS AND METHODS

### 2.1 | Isolation and culture of hNPCs

The study was conducted in accordance with the Declaration of Helsinki, and the protocol was approved by the Ethics Committee of Università Campus Bio-Medico di Roma (Rome, Italy) and National Cancer Institute (Vilnius, Lithuania) under approval numbers n. 09/15 PAR ComEt CBM and n. 2021/01-1301-779, respectively. For this study, human IVD tissues were obtained from 10 patients undergoing discectomy due to lumbar disc herniation at Fondazione Policlinico Universitario Campus Bio-Medico (Rome, Italy). Demographic information, operated levels, Pfirrmann grade of harvested IVDs, and allocation to different experiments are depicted in Table 1. All patients provided written informed consent for the collection and use of surgical waste material for research purposes. Upon arrival at the laboratory, surgical specimens were washed with sterile phosphate-buffered

**TABLE 1** Summary of characteristics of the donor IVD samples.

Patient ID	Age (years)	Sex	Level	Pfirschmann grade	Application
1	58	M	L5-S1	IV	Figures 4, 6A,B, 7A,B, 8B-D, 8F
2	39	F	L5-S1	IV	Figures 4, 5, 6A, 7A-D, 8D-F
3	47	M	L3-L4	III	Figures 5, 6A,B, 7C,D, 8A-C, 8E,F
4	55	F	L4-L5	III	Figures 4, 5, 6A, 8A-D,G
5	75	F	L4-L5	IV	Figures 4, 5, 7A, 8D,G
6	37	M	L4-L5	III	Figures 6B, 7A,B, 8A-D
7	53	F	L5-S1	III	Figures 4, 6B, 7A
8	67	F	L4-L5	IV	Figures 4, 6A,B, 7A,C,D, 8A,B,E,G
9	63	F	L4-L5	IV	Figures 7A, 8A,C
10	54	M	L4-L5	III	Figures 5, 7A, 8A,D

Note: Age, sex, operated levels, Pfirschmann grading, and experiment allocation are listed.  
Abbreviation: IVD, intervertebral disc.

saline (PBS) and minced into pieces 3–5 mm in diameter with sterilized scissors and scalpels, carefully separating the NP tissue as previously described.<sup>22</sup> Specimens were then digested overnight at 37°C under gentle agitation in sterile Dulbecco's Modification of Eagle's Medium High Glucose (DMEM; Corning, Corning, NY, USA) containing 1% penicillin/streptomycin, 1% glutamine (Sigma, St. Louis, MO, USA), 5% heat-inactivated fetal bovine serum (FBS; Gibco, batch no. 08F0597K) and 0.01% collagenase type II (Worthington, Lakewood, NJ, USA). FBS aliquots from the same batch were used in all serum-containing media utilized in this study. The digest was filtered through a 70-µm filter, the suspension was centrifuged at 300g for 5 min, and isolated cells were cultured in DMEM with 10% FBS, 1% P/S, 1% glutamine, and 25 µg/mL ascorbic acid (21% O<sub>2</sub>, 5% CO<sub>2</sub>, 37°C). Culture media were refreshed every 3 days, and cells were allowed to grow until reaching 80%–90% confluence.

## 2.2 | Isolation and characterization of Wharton's Jelly MSCs

Human WJ-MSCs were obtained and characterized by the National Cancer Institute of Vilnius (Lithuania). Healthy donors (delivering mothers aged between 18 and 44 years) provided informed consent for the use of cord tissue for research purposes. Different batches of WJ-MSCs at passages 4–6 (P4–P6) were obtained from one donor and seeded in DMEM Low Glucose containing 10% FBS, 2 mM L-Alanyl-L-Glutamine, and 40 µg/mL gentamicin at a density of  $4 \times 10^3$  cells/cm<sup>2</sup> on uncoated five-layer cell culture Multi-Flasks (Corning) and were cultured up to 70%–80% confluence. Then WJ-MSCs were washed three times using 50 mL PBS without Ca<sup>2+</sup> and Mg<sup>2+</sup>, and replenished with DMEM High Glucose without phenol red, 2 mM L-Alanyl-L-glutamine, 2% PRP lysate (PLTGold® Human Platelet Lysate, Sartorius, Göttingen, Germany), 2 IU/mL heparin, and 40 µg/mL gentamicin. Cells were cultured in standard conditions (21% O<sub>2</sub>, 5% CO<sub>2</sub>, 37°C) for 1–2 days. For the detection of cell surface markers, WJ-MSCs were characterized for positive expression of CD73, CD90, and CD105 and negative expression of SSEA3

markers using flow cytometry. A minimum of 25 000 cell events per assay were acquired using CytoFLEX (Beckman Coulter, Brea, CA, USA). Multilineage differentiation potential was evaluated following culture in osteogenic, adipogenic, and chondrogenic conditions, as previously described.<sup>23</sup> Briefly, osteogenic medium was composed of DMEM Low Glucose (Corning) containing 10% FBS, 0.1 µM dexamethasone, 0.2 mM ascorbic acid 2-phosphate, and 10 mM glycerol 2-phosphate. Adipogenic medium was prepared by combining DMEM Low Glucose (Corning) with 10% FBS, 1 µM dexamethasone, 0.5 mM 3-isobutyl-1-methylxanthine (IBMX), 10 µg/mL insulin, and 100 µM indomethacin. To reproduce chondrogenic conditions, WJ-MSCs were detached by trypsinization, centrifuged at 300g for 5 min to form a pellet, and then cultured in Chondrogenic Differentiation Medium (Lonza, Basel, Switzerland). After 21 days, Alizarin red staining and Oil Red O staining were performed on WJ-MSCs seeded in monolayer, to evaluate for osteogenic and adipogenic differentiation, respectively. Cell pellets were fixed in 10% neutral buffered formalin, paraffin-embedded, and stained with Alcian blue to assess chondrogenic differentiation. Microscopic observation was performed using a NanoZoomer 2.0RS (Hamamatsu Photonics, Hamamatsu, Japan) at 10X and 20X magnification. Six random fields per each histological section were digitally acquired and independently assessed by three blinded evaluators in terms of staining intensity of the ECM (Alizarin red and Alcian blue) or lipid-containing vacuoles (Oil Red O) to evaluate WJ-MSC multidifferentiation capacity.

## 2.3 | Isolation and characterization of WJ-MSCs derived EVs

After reaching 70%–80% confluency, WJ-MSCs were washed with PBS and cultured in serum-free medium for an additional 24 h at 37°C in an atmosphere of 5% humidified CO<sub>2</sub>. Conditioned medium was then collected and filtered through a 0.22 µm pore filter to remove cell debris. EVs were extracted from the filtered conditioned medium through tangential flow filtration using a VivaFlow 200 filter with a 100-kDa molecular weight cutoff (MWCO) and concentrated

10-fold (volume reduced 10-fold). Buffer was changed to PBS. The final product was sterile-filtered using a 220-nm filter. Measurement of nanoparticle number and size distribution of EVs were analyzed by nanoparticle trafficking analysis (NTA) using the NANOSIGHT NS300 system (Malvern, UK) according to the manufacturer's instructions. EV morphology was observed at transmission electron microscopy (TEM). Briefly, after isolation, EVs suspended in PBS were loaded onto formvar carbon-coated mesh copper grids for 10 min at room temperature. Adsorbed EVs were negatively stained with 1% phosphotungstic acid for 5 min. Finally, the air-dried EV-containing grids were observed by TEM.

## 2.4 | EV uptake by hNPCs

Purified WJ-MSC-derived EVs were labelled with PKH26 (Sigma-Aldrich) and hNPCs were stained by Hoechst 33258 (Life Technologies, Thermo Fisher Scientific, Waltham, MA, US), following the manufacturer's instructions. After being washed in PBS and centrifuged at 110 000g for 90 min, EVs were suspended in basal medium at a concentration of 100 µg/mL and co-incubated with hNPCs for 4 h at 37°C. Images of EV uptake were acquired using a confocal laser scanning microscope (Zeiss LSM700, Carl Zeiss, Jena, Germany).

## 2.5 | hNPC metabolic activity

MTT assay (Sigma) was performed to evaluate hNPC metabolic activity after EV treatment at 1, 10, 50, 100, and 200 µg/mL concentrations, according to the manufacturer's instructions. hNPCs ( $n = 5$ ) were transferred to 96-multiwell plates ( $5 \times 10^3$  cells/well). At 48 h after treatment, DMEM was supplemented with 100 µL of MTT (3-(4,5-Dimethylthiazol-2-yl)-2,5-diphenyltetrazolium bromide) reagent ( $c = 5$  mg/mL). After 4 h at 37°C, the MTT solution was removed, and formazan crystals were dissolved with 100 µL of DMSO for 15 min at 37°C. Absorbance was read at 570 nm with reference at 690 nm using a Tecan Infinite M200 PRO. Results were normalized to the control group, which was considered to have 100% mitochondrial activity.

## 2.6 | hNPCs encapsulation in alginate beads and EV treatment

hNPCs were then cultured in a three-dimensional system as previously described.<sup>24</sup> Briefly, adherent hNPCs at P2 were detached by trypsinization, washed, and centrifuged at 1200 rpm for 5 minutes. Then, cells were resuspended in 1.2% low-viscosity sterile pharmaceutical grade alginate solution (Pronova Biopolymer, Drammen, Norway) at  $4 \times 10^6$  cells/mL and dropped using a syringe with a 21-gauge needle into a 102 mmol/L calcium chloride solution to form semisolid beads. After 10 min of polymerization, beads were washed with saline and cultures were maintained in DMEM High Glucose with 10% FBS, 1% P/S, and 25 µg/mL ascorbic acid (21%

O<sub>2</sub>, 5% CO<sub>2</sub>, 37°C). After 2 weeks, hNPCs in alginate beads were treated with either DMEM with EV-free serum as control or 10, 50, or 100 µg/mL EVs. EV-free serum was obtained via FBS ultracentrifugation as previously described.<sup>25</sup> Briefly, FBS aliquots were ultracentrifuged at 110 000 g for 17 h, and the supernatant was then filtered through a 0.22-µm filter. Media were refreshed every 2 days.

## 2.7 | Cell count and viability

hNPCs in alginate beads ( $n = 5$ ) were incubated for 10 min at 4°C in 55 mmol/L sodium citrate, 30 mmol/L EDTA, 0.15 M NaCl, pH 6.8 to dissolve beads and analyze cell count and viability using a CytoFLEX instrument with CytExpert Software (v.2.1, Beckman Coulter). Cell count was assessed at 1, 4, 10, and 14 days and expressed as event/µL. To evaluate the effect of EV treatment on cell death, hNPCs ( $n = 5$ ) were stained with Fixable Viability Dye conjugated with eFluor780 fluorochrome (Affymetrix eBioscience, Thermo Fisher Scientific) after 24 h of treatment, using the gating strategy depicted in Figure 1. Similarly, cell viability was determined by analyzing membrane integrity with the LIVE/DEAD assay, following the manufacturer's instructions. Briefly, hNPCs in alginate beads ( $n = 5$ ) were incubated for 45 min with ethidium homodimer-2 and calcein acetoxymethylester (AM) at room temperature, washed three times with PBS and incubated with Hoechst 33258 (Life Technologies) to stain the nuclei. After incubation, green, red, and blue fluorescence were detected using a confocal laser scanning microscope (Zeiss LSM700, Carl Zeiss).<sup>26</sup>

## 2.8 | Assessment of hNPC nitrite concentration

The Griess reaction was performed to measure nitrite concentration in the supernatant as an indicator of the production of nitric oxide (NO). Nitrites in the medium react with sulfanilic acid under acidic conditions forming a purple azo product which subsequently links to the naphthyl-ethylenediamine dihydrochloride suspended in water. After 1 week, supernatant samples from treated hNPCs and controls ( $n = 5$ ) were incubated with 20 µL Griess reagent (Invitrogen, Carlsbad, CA, USA) for 30 min in the dark, according to the manufacturer's instructions. Absorbance was then measured at 546 nm using a Tecan Infinite M200 PRO and nitrite concentration was calculated using a standard curve as the reference. Results were normalized to the control group.

## 2.9 | 1,9-dimethylmethylene blue (DMMB) assay

After 7 days of treatments, alginate beads were dissolved, and hNPC pellets ( $n = 8$ ) were digested overnight at 65°C with 100 µL papain (Sigma) in 0.25 mg/mL in 50 mM phosphate buffer (pH 1.5), containing 5 mM cysteine-hydrochloride and 5 mM ethylenediaminetetraacetic acid. GAGs were measured by reaction with DMMB



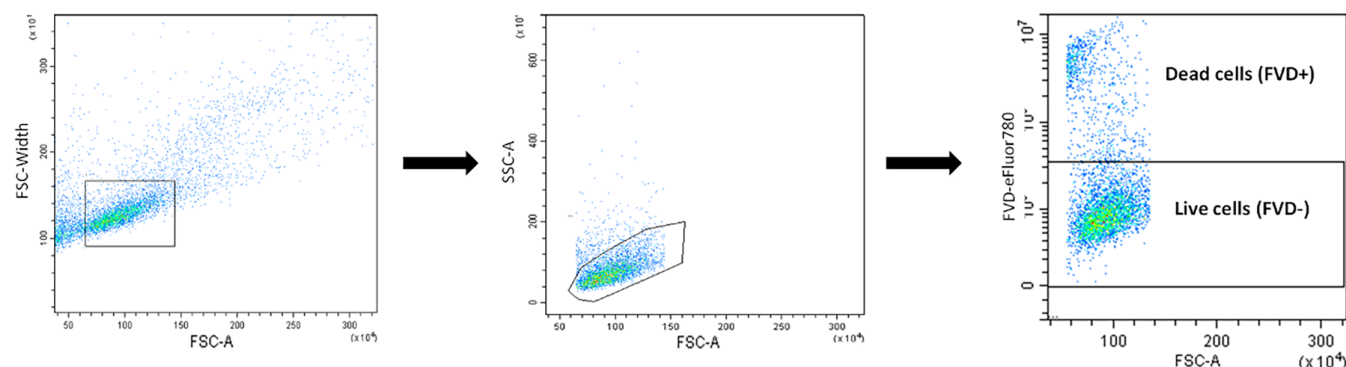


**FIGURE 1** Gating strategy to evaluate hNPC viability. Cells were stained with Fixable Viability Dye conjugated with eFluor780 fluorochrome to exclude dead cells (FVD+). Gating strategy based on Forward and Side scatter is shown. FVD, fixable viability dye; hNPC, human nucleus pulposus cells.

(Polysciences, Warrington, PA, USA) using chondroitin sulfate (Sigma) as a standard. Absorbance measurements were performed at 530 nm (Tecan Infinite M200 PRO). Data were expressed as GAG quantity normalized to DNA content and comparing the percent variation between the control group (considered as the baseline) and the experimental groups. DNA content was assessed with PicoGreen assay (Invitrogen), using a standard curve based on known DNA concentrations. Fluorescence was measured at 488 nm and 520 nm wavelengths using a microplate reader (Tecan Infinite M200 PRO).

## 2.10 | Histological assessment

After 7 days of treatments, alginate beads were fixed in 10% (v/v) phosphate-buffered formalin (Sigma), embedded in paraffin, and cut in 5- $\mu$ m sections, according to standard procedures. Slides of consecutive sections were dewaxed, rehydrated, and stained with hematoxylin-eosin (HE) and Alcian Blue to assess cell morphology and proteoglycan content, respectively. Microscopic observation was performed using a NanoZoomer 2.0RS (Hamamatsu Photonics, Hamamatsu, Japan) at 10X and 20X magnification.

## 2.11 | RNA extraction and gene expression analysis

After 7 days of treatment, alginate beads were digested and total RNA was extracted from pellets using TRIzol reagent (Invitrogen). cDNA was synthesized using High-Capacity cDNA Reverse Transcription kit (Applied Biosystems, Foster City, CA, USA) according to the manufacturer's instructions. mRNA levels of aggrecan (*ACAN*;  $n = 3$ , Hs0153936), matrix metalloproteinase (*MMP*)-1 ( $n = 6$ , Hs00899658), *MMP*13 ( $n = 6$ , Hs00233992), a disintegrin and metalloproteinase with thrombospondin motifs (*ADAMTS*)-5 ( $n = 6$ , Hs00199841), SRY-Box Transcription Factor (*SOX*)-9 ( $n = 3$ , Hs01001343), *IL*6 ( $n = 6$ , Hs00174131), nitric oxide synthase (*NOS*)-2 ( $n = 5$ , Hs01075529), and glyceraldehyde-3-phosphate dehydrogenase (*GAPDH*, Hs03929097) were measured through qRT-PCR using TaqMan Gene Expression Assays and TaqMan Universal

Master Mix II with UNG on a 7900HT FAST Real Time PCR System. qRT-PCR analysis for keratin (*KRT*)-19 ( $n = 3$ , Forward: 5'-AACGGC-GAGCTAGAGGTGA-3'; Reverse: 5'-GGATGGTCGTGTAGTAGTGGC-3') and *GAPDH* (Forward: 5'-GAAGGTGAAGGTCCGAGT-3'; Reverse: 5'-GAAGATGGTGATGGGATTTC-3') was performed using SYBR Green Master Mix (Applied Biosystems). The expression of each gene has been normalized to *GAPDH* expression and calculated as  $2^{-\Delta\Delta C_t}$ . Gene expression levels were normalized to levels measured in the control group, which was considered as a baseline.

## 2.12 | Western Blot analysis

Total proteins were isolated from WJ-MSC, hNPC and WJ-MSC-derived EV lysates using the radioimmunoprecipitation assay buffer (RIPA buffer; Sigma) for 30 min on ice, cleared by centrifugation for 30 min at 12 000 g at 4°C for 30 min and quantified using the detergent compatible (DC) protein assay kit (Bio-Rad, Hercules, CA, USA). Each sample was loaded on 4%-12% SDS-PAGE gels, transferred onto nitrocellulose membranes through the Trans-Blot Turbo Transfer System (Bio-Rad) and incubated in a blocking buffer (TBST 1X with 5% nonfat dry milk) for 1 h. Membranes were incubated with a primary antibody overnight shaking at 4°C in TBST 1X with 1% nonfat dry milk. Anti-CD63 (mouse, 1:1000, Invitrogen), anti-CD9 (mouse, 1:1000, Invitrogen), anti-TSG101 (mouse, 1:1000, Invitrogen), and anti-GRP75 (rabbit, 1:2000, Proteintech, Thermo Fisher Scientific), anti-COL1A1 (rabbit, 1:1000; Abcam), anti-COL2A1 (rabbit, 1:1000, Abcam), and anti-tubulin (1:5000, Abcam, Cambridge, UK) primary antibodies were utilized. Anti-mouse and anti-rabbit HRP-conjugated antibodies (1:10000, Abcam) were used and chemiluminescence signals were detected using ChemiDoc (Bio-Rad) and Quantity One software (Bio-Rad) to quantify the signal intensity of different bands.

## 2.13 | Statistical analysis

All quantitative data are expressed as means  $\pm$  standard deviations (SD). The normality of data distribution was determined with the Wilk-Shapiro test. Statistical analysis of the results was performed using

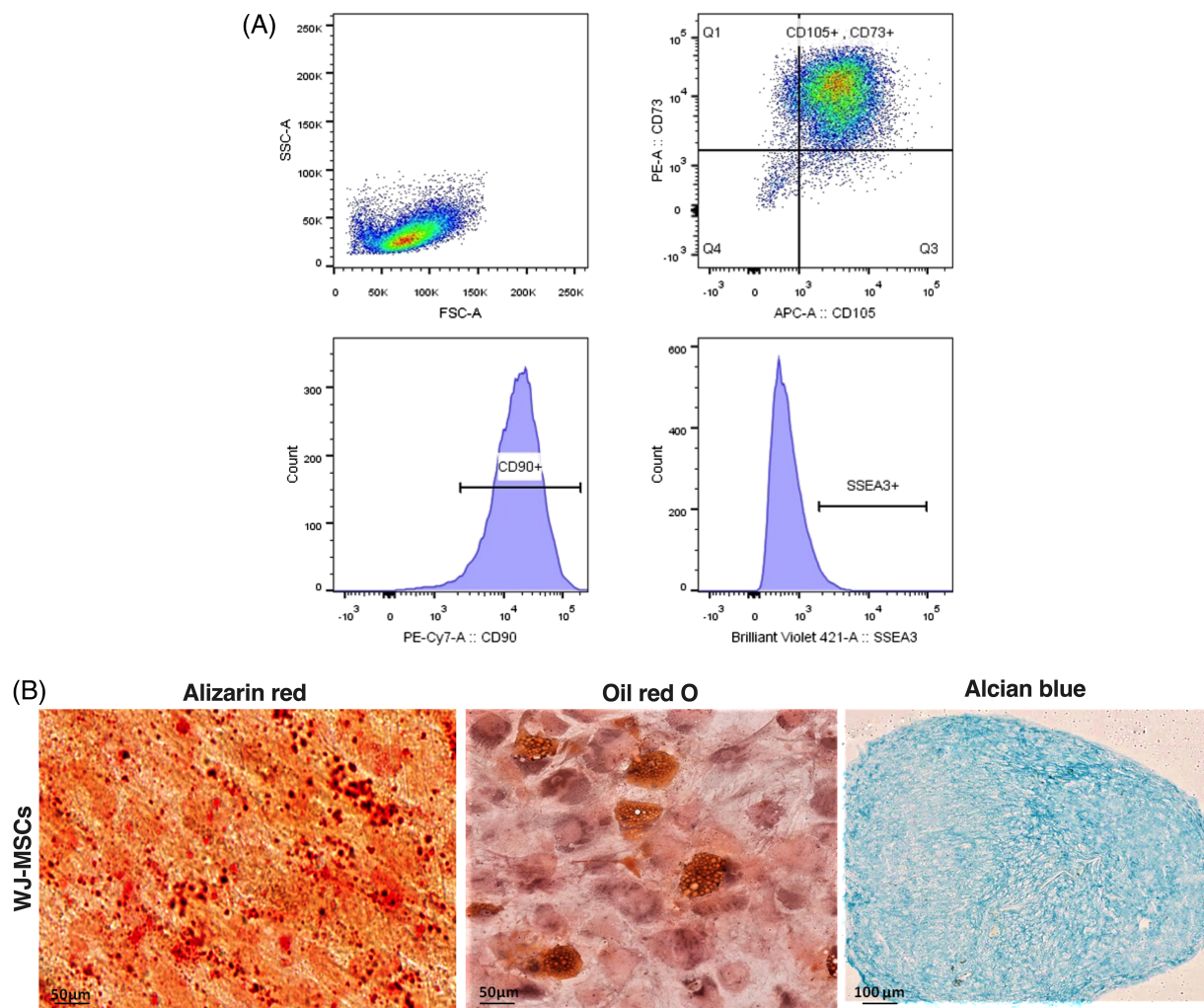


**FIGURE 2** Characterization of WJ-MSCs. (A) Cell surface markers (CD90, CD105, CD73, and SSEA3) detected by flow cytometric analysis. (B) Multilineage differentiation of WJ-MSCs towards the osteogenic, adipogenic, and chondrogenic lineages was confirmed by Alizarin Red, Oil red O, and Alcian Blue staining of WJ-MSC pellets (left and center, scale bar: 50  $\mu$ m; right, scale bar: 100  $\mu$ m). WJ-MSCs, Wharton's Jelly mesenchymal stromal cells.

one-way or two-way analysis of variance (ANOVA) with Dunnett's or Tukey's post-tests for multiple comparisons wherever applicable. Statistical significance was set as  $p < 0.05$ . Formal analysis was performed using Prism 8 (GraphPad, San Diego, CA, USA). Three technical replicates were performed in each experiment. Representative data are shown.

### 3 | RESULTS

#### 3.1 | WJ-MSC characterization

Flow cytometric analysis showed that WJ-MSCs were positive for CD90 (97.2%), CD73 (92.6%), and CD105 (93.4%), while being negative for SSEA3 (4.78%; Figure 2A), thence confirming their MSC phenotype. Multilineage differentiation was confirmed by calcium deposits stained by Alizarin red after osteogenic differentiation, lipid droplets stained by

Oil red O after adipogenic differentiation, and GAG stained by Alcian blue following chondrogenic differentiation (Figure 2B).

#### 3.2 | WJ-MSC-EV identification and characterization

Following isolation, EV concentration was  $1.60 \times 10^9$  particles/mL with a mean particle diameter of 172.5 nm, according to NTA (Figure 3A). The typical EV morphology of these particles was confirmed by TEM analysis (Figure 3B). According to WB results, protein expression of EVs surface markers TSG101, CD9, and CD63 was higher in EVs samples compared to cell lysates (Figure 3C). Fluorescent microscopy observation of PKH26-labeled EVs co-incubated with hNPCs showed internalization of vesicles throughout the perinuclear region of recipient cells, indicating that the nano-sized vesicles were uptaken by hNPCs (Figure 3D).

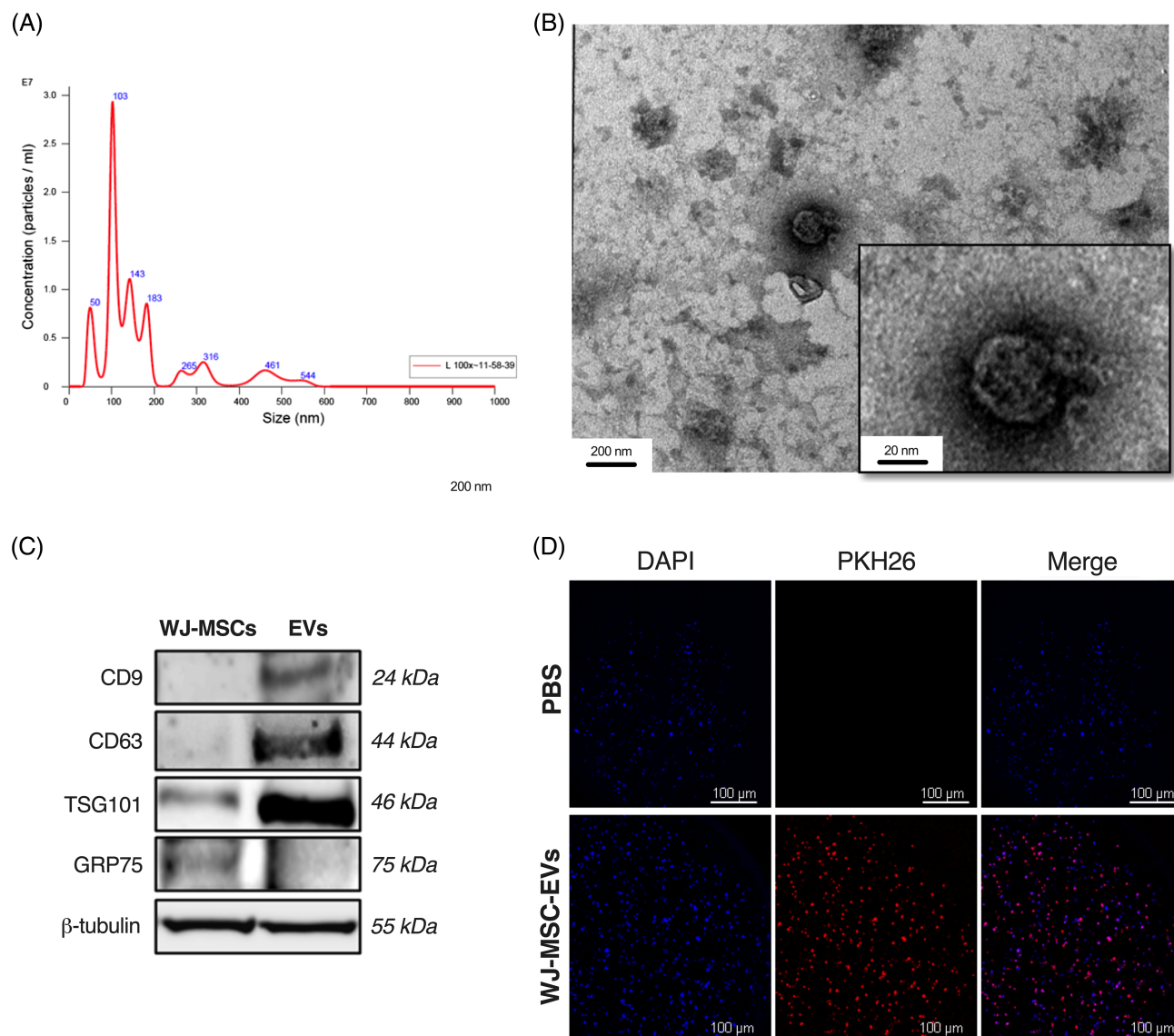


**FIGURE 3** Identification and characterization of WJ-MSC-EVs. (A) Particle size distribution of WJ-MSC-EVs measured by NTA. (B) TEM imaging showed the typical EV morphology in WJ-MSC-EV samples (left, scale bar: 200 nm; right box, scale bar: 20 nm). (C) WB analysis of EV protein markers CD63, CD9, and TSG101. (D) Representative images of hNPCs incubated with PBS or PKH26-labeled WJ-MSC-EVs (red). hNPC nuclei were stained with DAPI (blue). Magnification: 20× scale bar: 100 μm. DAPI, 4',6-diamidino-2-phenylindole, EVs, extracellular vesicles, hNPCs, human nucleus pulposus cells, NTA, nanoparticle trafficking analysis, PBS, phosphate-buffered saline, TEM, transmission electron microscopy, WB, Western blot, WJ-MSCs, Wharton's Jelly mesenchymal stromal cells.

### 3.3 | WJ-MSC-EVs improved hNPC metabolic activity

To evaluate the most effective WJ-MSC-EV concentration on hNPCs, a dose-response experiment was performed to assess the effect of increasing WJ-MSC EVs on hNPC metabolic activity measured with the MTT assay. Interestingly, significant differences were encountered following treatments with 10 μg/mL ( $129.6 \pm 10.05\%$ ;  $p < 0.01$ ) and 100 μg/mL ( $140.2 \pm 19.25\%$ ;  $p < 0.05$ ) WJ-MSC-EVs compared to the control group (Figure 4). Although a substantial increase was also reported in the group treated with 50 μg/mL WJ-MSC-EVs

( $122.4 \pm 17.88\%$ ), no statistically significant difference was found when compared to control.

### 3.4 | WJ-MSC-EVs promoted cell proliferation and viability

Flow cytometry was used to assess cell viability and the presence of proliferating cells following WJ-MSC-EV treatment at different doses. Results revealed an increase in cell content at 10 and 14 days after starting 3D cell culture (Figure 5A). Specifically, at day 10, exposure to

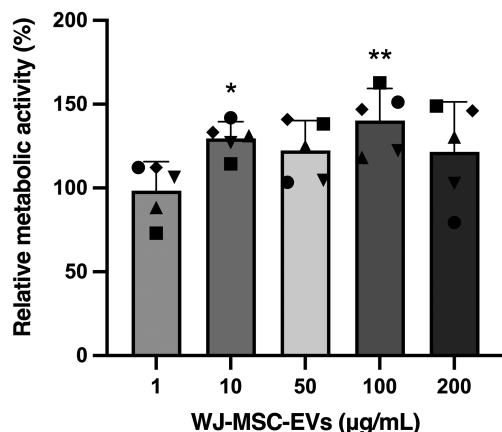


**FIGURE 4** MTT assay for hNPC metabolic activity assessment. WJ-MSC-EVs significantly improved metabolic activity in the experimental group treated with 10 µg/mL and 100 µg/mL. Data are expressed as percent variation between the control and experimental groups ( $n = 5$ ). \* $p < 0.05$ , \*\* $p < 0.01$  compared to the control group. hNPCs, human nucleus pulposus cells; WJ-MSC-EVs, Wharton's Jelly mesenchymal stromal cell-derived extracellular vesicles.

10 and 50 µg/mL WJ-MSC-EVs led to a statistically significant increase of cell count ( $218.9 \pm 16.58$  cells/µL and  $224.7 \pm 18.49$  cells/µL,  $p < 0.01$  and  $p < 0.05$  respectively). At day 14, mean hNPCs content remained significantly higher after treatment with 50 µg/mL WJ-MSC-EVs ( $250.2 \pm 22.69$  cells/µL;  $p < 0.001$ ) compared to the control group. Likewise, cell concentration in the 50 µg/mL group was significantly higher than the 100 µg/mL group ( $p < 0.05$ ) at both 10 and 14 days. Although 10 and 100 µg/mL WJ-MSC-EV treatments were not associated with a statistically significant higher cell count at day 14, cell content still showed an increasing trend compared to the control group.

Furthermore, WJ-MSC-EVs were able to improve hNPC viability (Figure 5B). After 1 day, dead cell exclusion was performed with Fixable Viability Dye conjugated with eFluor780 fluorochrome through flow cytometry and significantly lower numbers of dead cells were detected after treatment with 10 and 100 µg/mL WJ-MSC-EVs ( $7.26 \pm 8.83\%$  and  $7.73 \pm 8.99\%$ , respectively) compared to controls ( $10.3 \pm 8.78$ ,  $p < 0.05$ ). These results were confirmed by live/dead staining of hNPCs encapsulated in alginate beads as showed in Figure 5C.

### 3.5 | WJ-MSC-EVs attenuated nitrite-induced oxidative stress

Compared to the control group, NOS-2 mRNA levels were significantly lower in the 100 µg/mL group ( $0.24 \pm 0.15$ ) compared to the control group ( $p < 0.001$ ; Figure 6A). Endogenous nitrite release into the supernatant by hNPCs was detected by Griess reaction (Figure 6B). Interestingly, nitrite levels were significantly lower following exposure to 50 and 100 µg/mL WJ-MSC-EVs ( $p < 0.05$  and  $p < 0.01$ , respectively), with nitrite concentration fold-changes being

$1.01 \pm 0.31$  in the 10 µg/mL group,  $0.75 \pm 0.15$  in the 50 µg/mL group, and  $0.59 \pm 0.12$  in the 100 µg/mL group.

### 3.6 | WJ-MSC-EVs enhanced ECM production

To investigate the role of WJ-MSC-EVs on ECM production, DMMB assay and Alcian blue staining were performed. DMMB colorimetric assay resulted in an enhancement of GAG production normalized to DNA. Indeed, three-dimensional hNPC cultures treated with all WJ-MSC-EV concentrations under investigation showed significantly higher levels of GAG compared to control, in a dose-dependent manner (10 µg/mL:  $123.0 \pm 19.43\%$ ,  $p < 0.05$ ; 50 µg/mL:  $143.2 \pm 28.91\%$ ,  $p < 0.01$ ; 100 µg/mL:  $174.2 \pm 40.12\%$ ,  $p < 0.01$ ; Figure 7A). Alcian blue staining qualitatively confirmed these results, showing that WJ-MSC-EVs may promote ECM synthesis in degenerated hNPCs. In addition, WB analysis also demonstrated a significant increase of collagen type II (Figure 7C) in hNPCs treated with 50 µg/mL WJ-MSC-EVs ( $1.43 \pm 0.21$ ) compared to the control ( $p = 0.009$ ) and cells treated with 10 µg/mL EVs ( $0.98 \pm 0.02$ ). Intriguingly, WJ-MSC-EVs also decreased the content of collagen type I (Figure 7D) in a dose-dependent fashion, which was statistically significant when comparing the 100 µg/mL group ( $0.35 \pm 0.08$ ) with the control ( $p = 0.002$ ), 10 µg/mL ( $1.03 \pm 0.16$ ,  $p = 0.002$ ), and 50 µg/mL groups ( $0.73 \pm 0.22$ ,  $p = 0.04$ ).

### 3.7 | WJ-MSC-EVs maintained hNPCs phenotype and blunted inflammatory and ECM catabolic marker expression

WJ-MSC-EVs significantly reduced the expression of ADAMTS-5, MMP-1, and MMP-13 genes. More specifically, ADAMTS-5 mRNA levels (Figure 8A) significantly decreased following treatment with all investigated WJ-MSC-EV doses (10 µg/mL:  $0.18 \pm 0.16$ ,  $p < 0.001$ ; 50 µg/mL:  $0.29 \pm 0.19$ ,  $p < 0.001$ ; 100 µg/mL:  $0.42 \pm 0.34$ ,  $p < 0.05$ ). Similarly, MMP-1 gene expression (Figure 8B) was downregulated by 50 and 100 µg/mL WJ-MSC-EVs ( $0.267 \pm 0.26$ ,  $p < 0.01$ ; 100 µg/mL:  $0.208 \pm 0.19$ ,  $p < 0.001$ , respectively). Likewise, a statistically significant decrement of MMP-13 expression (Figure 8C) was noted after exposure to all WJ-MSC-EV concentrations (10 µg/mL:  $0.34 \pm 0.25$ ,  $p < 0.01$ ; 50 µg/mL:  $0.47 \pm 0.38$ ,  $p < 0.05$ ; 100 µg/mL:  $0.63 \pm 0.27$ ,  $p < 0.05$ ). Moreover, WJ-MSC-EVs were able to significantly blunt IL-6 gene expression (Figure 8D) after exposure to 10 and 50 µg/mL ( $0.29 \pm 0.205$ ,  $p < 0.001$ ;  $0.26 \pm 0.204$ ;  $p < 0.001$ , respectively). Interestingly, compared to the control group, WJ-MSC-EV-treated hNPCs expressed significantly higher ACAN, SOX-9, and KRT19 mRNA levels. Indeed, hNPCs displayed an increased mRNA expression of ACAN (Figure 8E) after treatment with 50 µg/mL WJ-MSC-EVs ( $2.2 \pm 0.30$ ;  $p < 0.05$ ), while both SOX-9 (Figure 8F) and KRT19 (Figure 8G) expression levels were significantly higher after treatment with 10 µg/mL WJ-MSC-EVs compared to the control ( $4.74 \pm 0.36$ ;  $p < 0.01$  and  $1.34 \pm 0.06$ ;  $p < 0.05$ , respectively).



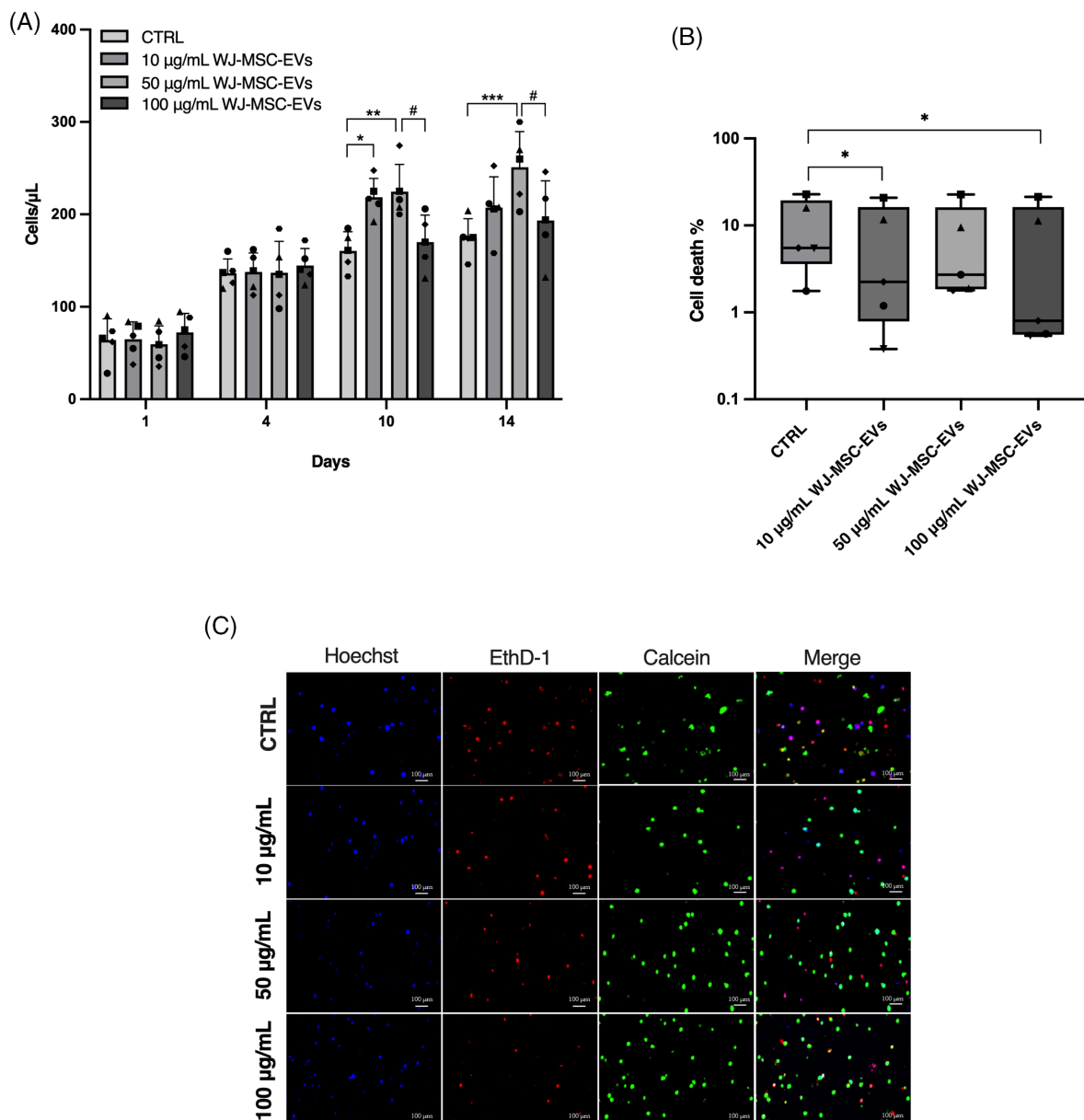


**FIGURE 5** WJ-MSC-EVs promoted hNPCs proliferation and viability. (A) Cell count significantly increased after treatment with 10 and 50  $\mu\text{g/mL}$  WJ-MSC-EVs at day 10 and 14, as compared with the control group ( $n = 5$ ). (B) After 1 day, WJ-MSC-EV treatment significantly reduced hNPC death at 10 and 100  $\mu\text{g/mL}$  ( $n = 5$ ). (C) Live/Dead staining showed reduced cell death in hNPCs treated with WJ-MSC-EVs compared to control ( $n = 5$ ). Magnification: 20 $\times$ , scale bar: 100  $\mu\text{m}$ . \* $p < 0.05$ , \*\* $p < 0.01$ , \*\*\* $p < 0.001$  compared to the control group. # $p < 0.05$  compared to the 100  $\mu\text{g/mL}$  group. AM, acetoxymethyl ester; hNPCs, human nucleus pulposus cells; WJ-MSC-EVs, Wharton's Jelly mesenchymal stromal cell-derived extracellular vesicles.

## 4 | DISCUSSION

This study highlights the regenerative effect of WJ-MSC-EVs on hNPCs in vitro using a 3D alginate-bead culture model. Indeed, we showed that WJ-MSC-EVs improved hNPC metabolic activity, proliferation, and viability while reducing oxidative stress and expression of catabolic markers. Furthermore, treated hNPCs also displayed a higher abundance of GAG production as well as increased ECM and NPC marker expression.

Preclinical and preliminary clinical evidence has shown that intradiscal injection of MSCs may effectively replenish NP cell content and increase ECM metabolism while being safe and minimally invasive.<sup>9</sup> However, this promising therapeutic tool is likely limited by the hostile environment of the degenerative IVD, which seriously threatens transplanted cell viability and fate.<sup>19,27,28</sup> Recent evidence has suggested that the therapeutic benefits of MSCs are mainly mediated by paracrine mechanisms.<sup>29,30</sup> Therefore, the identification of the MSC secretome is gaining significant momentum in the field.



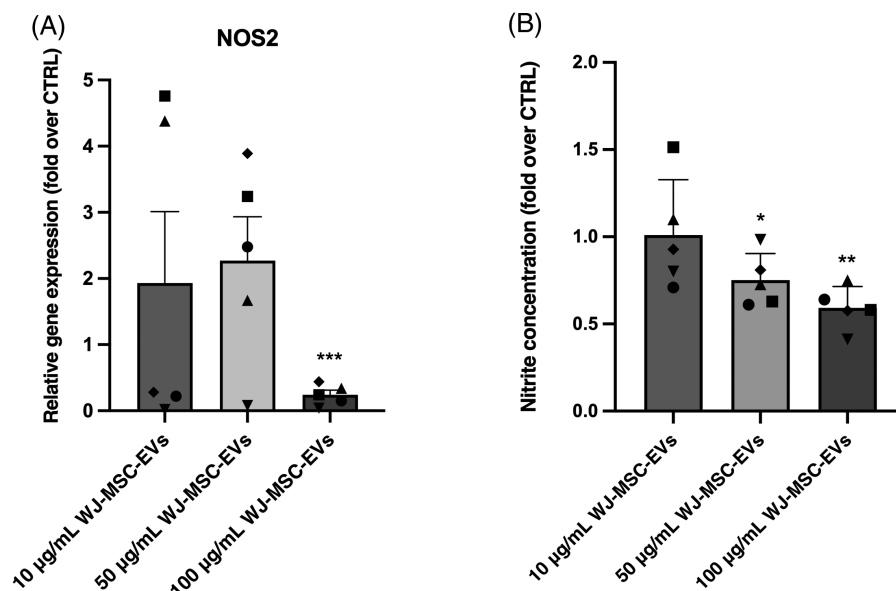


**FIGURE 6** (A) NOS2 mRNA levels were significantly reduced by 100 µg/mL WJ-MSC-EVs ( $n = 5$ ). WJ-MSC-EVs led to a significant decrease of nitrite concentration (B) released in cell culture supernatant after treatment with 50 and 100 µg/mL WJ-MSC-EVs compared to the control group ( $n = 5$ ). \* $p < 0.05$ , \*\* $p < 0.01$ , \*\*\* $p < 0.001$  compared to the control group. hNPCs, human nucleus pulposus cells; NOS2, nitric oxide synthase 2; WJ-MSC-EVs, Wharton's Jelly mesenchymal stromal cell-derived extracellular vesicles.

Among secreted factors, EVs have attracted particular attention due to their role as messengers and delivery systems between cells. Moreover, the EV cargo reflects the pathophysiological state of the donor cell, therefore consequently modulating target cell response.<sup>31</sup>

In our study, treatment with three different WJ-MSC-EV concentrations promoted the viability of hNPCs encapsulated in alginate beads after 24 h as well as proliferation at 10 and 14 days following exposure to low (10 µg/mL) and intermediate (50 µg/mL) EV doses. Previous studies have reported that EVs isolated from BM-MSCs increased the proliferation of hNPC pellets from day 7 to day 28.<sup>32</sup> Likewise, 50 µg/mL BM-MSC-derived exosomes significantly improved the proliferation rate of degenerated NPCs after 12 days, underlying that their effect was more effective compared to indirect co-culture of BM-MSCs and NPCs.<sup>33</sup>

Oxidative stress is another major trigger of IDD. Our results demonstrated that WJ-MSC-EVs were able to decrease the release of nitrites along with NOS2 gene expression, while also improving mitochondrial metabolism of hNPCs. According to Xia et al.,<sup>34</sup> MSC-derived exosomes restored mitochondrial dysfunction caused by oxidative stress and improved cellular homeostasis by replacing damaged mitochondrial components and delivering proteins with antioxidant function. Similarly, Liao et al.<sup>35</sup> demonstrated that MSC-derived exosomes ameliorated advanced glycation end products (AGEs)-induced endoplasmic reticulum stress in IVD cells both in vitro and in a rat tail model.

ECM anabolism and remodelling is a crucial response to foster IVD endogenous repair following injury or degenerative insults.<sup>36</sup> In this study, WJ-MSC-EVs were able to increase GAG production in a dose-dependent fashion as confirmed by DMMB assay and Alcian blue staining. Furthermore, hNPCs treated with WJ-MSC-EVs also showed an increase in collagen type II and a decrease in collagen type I content. GAGs and proteoglycans constitute the supporting structure of the ECM, while collagen type II is the second most abundant matrix component of the NP, which collectively help preserve IVD

integrity and biomechanics. Nonetheless, IDD is characterized by the progressive loss of collagen type II and gradual replacement with collagen type I, which renders the NP stiffer and more fibrotic.<sup>6</sup> Unbalanced expression of matrix-degrading enzymes such as MMPs or tissue inhibitors of metalloproteinases (TIMPs) may disrupt the ECM. Indeed, clinical studies showed that MMP-1 serum levels were significantly higher in patients with severe IDD compared to subjects with mild or moderate IDD. Interestingly, it has been reported that after stimulation of NPCs with BM-MSC-derived exosomes, TIMP-1 expression was increased while MMP-1 and MMP-3 were downregulated.<sup>33</sup> In our experimental conditions, gene expression analysis suggested that WJ-MSC-EVs were able to significantly reduce mRNA levels of catabolic enzymes MMP-1, MMP-13, ADAMTS-5, and the proinflammatory cytokine IL-6, which are all involved in the pathogenesis of IDD. Indeed, the inflammatory environment of IDD significantly impairs cell survival.<sup>37</sup> Previous studies have highlighted the anti-inflammatory role of exosomes derived from BM-MSCs, which proved to attenuate H<sub>2</sub>O<sub>2</sub>-induced inflammation in NPCs by suppressing inflammatory mediators and activation of the NLR family pyrin domain containing 3 (NLRP3) inflammasome. These results were also confirmed in vivo in a rabbit model, suggesting the possibility of using EVs as a novel therapeutic strategy for IVD regeneration.<sup>34</sup> In our study, we also analyzed mRNA levels of the NPC phenotypic markers ACAN, KRT19, and SOX-9. Intriguingly, EV-treated cells showed a higher expression level of such genes compared to the untreated group. This may be also due to the gelatinous three-dimensional microenvironment established by alginate bead culture, which has been demonstrated to support the maintenance of a healthy NPC phenotype.<sup>38</sup>

In the last decade, the EV research field has been actively focused on vesicle-mediated intercellular paracrine interactions, which may be applied to the development of drug delivery systems as well as biomarkers in the screening of different disorders.<sup>39</sup> Compared to cell therapy, an alternative approach based on MSC-derived EVs exhibits

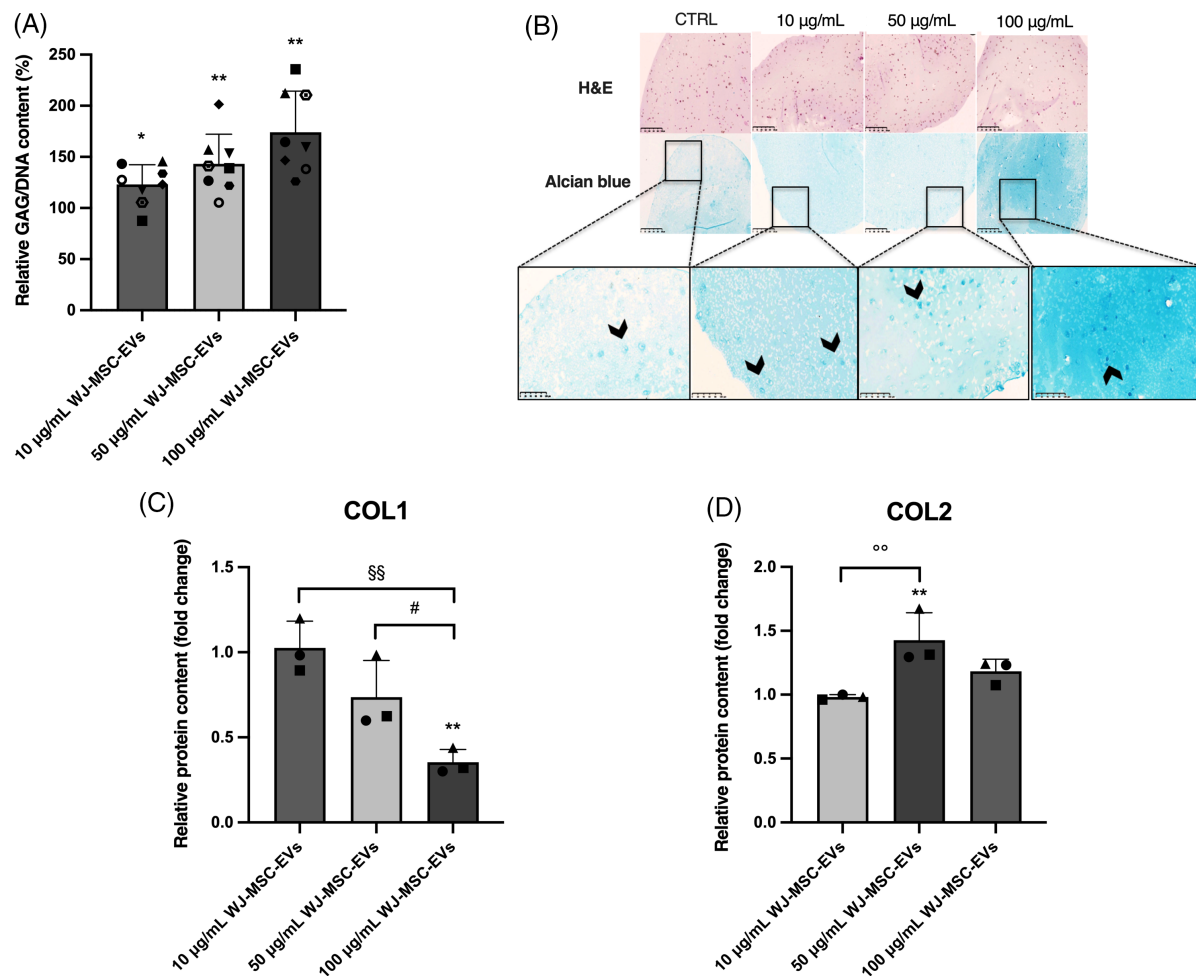


**FIGURE 7** WJ-MSC-EVs enhanced ECM synthesis in treated hNPCs. (A) GAG/DNA ratio in hNPCs after WJ-MSC-EVs treatment demonstrated a significant dose-dependent increase in all experimental groups (10, 50, and 100 µg/mL WJ-MSC-EVs). Data are expressed as GAG/DNA ratio percent variation between the control and experimental groups ( $n = 8$ ). \* $p < 0.05$ , \*\* $p < 0.01$  compared to the control group. (B) Alcian Blue staining of hNPC alginate beads. Representative images are shown. Blue color indicates proteoglycans. Arrowheads point to proteoglycan deposits. Upper rows, scale bar: 500 µm; bottom boxes, scale bar: 100 µm. hNPCs treated with 50 and 100 µg/mL WJ-MSC-EVs showed a significant increase of COL2 (C) and a decrease of COL1 (D) content, respectively ( $n = 3$ ). COL, collagen; GAG, glycosaminoglycans; hNPCs, human nucleus pulposus cells; WJ-MSC-EVs, Wharton's Jelly mesenchymal stromal cell-derived extracellular vesicles. \*\* $p < 0.01$ , compared to the control group. °° $p < 0.01$  compared to the 10 µg/mL group. §§ $p < 0.01$  compared to the 50 µg/mL group. # $p < 0.05$  compared to the 100 µg/mL group.

evident advantages such as low immunogenicity and cytotoxicity, permeability of biological barriers, and no concern for tumorigenesis. In addition, the role of drug- or biomaterial-loaded EVs or engineered EVs is being increasingly explored. Collectively, all these characteristics may render EVs the ideal natural carrier for the development of nanomedicine tools.<sup>40</sup> Furthermore, the therapeutic potential of EVs mainly depends on their intrinsic cargo composed of RNA, DNA, lipids, and proteins. miRNAs are described among the main mediators of EV capability to regulate cell response by stimulating or inhibiting the post-transcriptional process of target genes.<sup>31</sup> Cheng et al.<sup>41</sup> highlighted the anti-apoptotic effect of miR-21 in tumor necrosis factor (TNF)- $\alpha$  treated NPCs. In their study, miR-21 was able to down-regulate the pro-apoptotic *PTEN* gene causing the activation of the phosphoinositide 3-kinase (PI3K)/Akt signaling pathway, thus

stimulating NPC proliferation, regulating cell survival, and inhibiting apoptosis. However, several critical EV characteristics still need to be elucidated, including biodistribution, pharmacokinetics, pharmacodynamics, optimal route of administration (local or systemic), dosage, and timing of harvest.<sup>42</sup> Therefore, further studies are needed to clarify their mechanism of action. Furthermore, optimization of isolation and purification methods according to good manufacturing practices and translation to the clinical practice remain even more challenging.<sup>13</sup>

This study was the first to investigate the use of WJ-MSC-derived EVs on an in vitro model of IDD. Compared to other MSC types, WJ-MSCs offer several additional advantages, such as prompt availability in blood banks, non-invasive harvesting, low incidence of graft vs. host disease, and the consequent

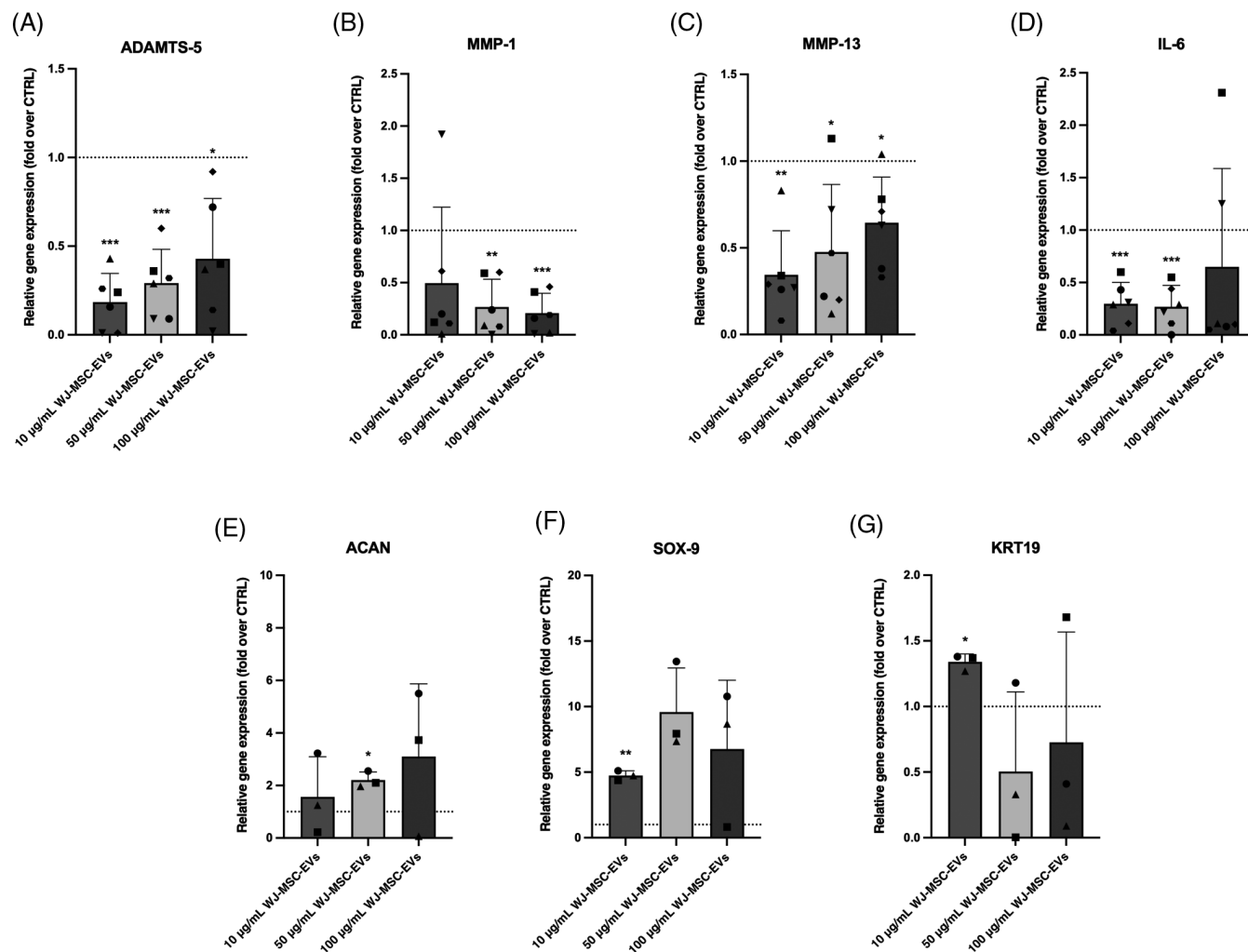


**FIGURE 8** WJ-MSC-EVs maintained hNPC phenotype and reduced catabolic gene expression. WJ-MSC-EV treatment resulted in a significant decrease of ADAMTS5 (A), MMP1 (B), MMP13 (C), and IL6 (D) mRNA levels, while increasing ACAN (E), SOX9 (F) and KRT19 (G) gene expression. Results were normalized based on GAPDH expression and calculated as fold change compared to the controls. See Materials and Methods for sample size. \* $p < 0.05$ , \*\* $p < 0.01$ , \*\*\* $p < 0.001$ , \*\*\*\* $p < 0.0001$  compared to the control group. ACAN, aggrecan; ADAMTS, a disintegrin and metalloproteinase with thrombospondin motifs; hNPCs, human nucleus pulposus cells; IL, interleukin; MMP, matrix metalloproteinase; NOS, nitric oxide synthase; SOX, SRY-box transcription factor; WJ-MSC-EVs, Wharton's Jelly mesenchymal stromal cell-derived extracellular vesicles.

possibility to manufacture allogeneic products.<sup>19</sup> In this regard, large-scale production and distribution of WJ-MSC-EV-based products may be more efficient and cost-effective compared to the use of MSCs isolated from adult tissues. However, this study has several limitations. First, results have been obtained through an in vitro experimental design. Although hNPCs showed to strongly respond to EVs, the EV cargo has not been specifically characterized and investigated. Moreover, despite significant results, gene expression data should be confirmed at the protein level to better define the biological effects of WJ-MSC-derived EVs on hNPCs. Second, hNPCs have been harvested from herniated disc tissues without correlating the results with the severity of IDD, which may impact their biological response to EVs. Third, we used a 3D culture model that may re-differentiate hNPCs to a healthy phenotype, thence independently influencing hNPC

response. Furthermore, as hNPCs were cultured in physiologic conditions, the putative anti-inflammatory effect of WJ-MSC-derived EVs remains speculative until proven under proinflammatory experimental conditions.

## 5 | CONCLUSION

In this study, we demonstrated that EVs isolated from WJ-MSCs increased hNPC proliferation, metabolic activity, ECM production and reduced cell death and inflammation. These results indicate that EVs may represent a novel cell-free strategy for IVD repair and regeneration. Moreover, considering their multiple advantages and functions, EVs may emerge as an innovative tool for the development of nano-medical treatments.

## ACKNOWLEDGMENTS

This research received funding from the European Union's Horizon 2020 Research and Innovation Programme under grant agreement No. 732163 and the European Union - Next Generation EU - NRRP PNC-E3-2022-23683269 PNC-HLS-TA.

## CONFLICT OF INTEREST STATEMENT

GV is an Editorial Board member of JOR Spine and co-author of this article. He was excluded from editorial decision-making related to the acceptance of this article for publication in the journal.

## ORCID

Gianluca Vadalà  <https://orcid.org/0000-0001-7142-1660>

Luca Ambrosio  <https://orcid.org/0000-0003-2424-1274>

## REFERENCES

- Vos T, Flaxman AD, Naghavi M, et al. Years lived with disability (YLDs) for 1160 sequelae of 289 diseases and injuries 1990-2010: a systematic analysis for the global burden of disease study 2010. *Lancet*. 2012;380:2163-2196.
- Russo F, Ambrosio L, Ngo K, et al. The role of type I diabetes in intervertebral disc degeneration. *Spine (Phila Pa 1976)*. 2019;44:1177-1185.
- Cannata F, Vadalà G, Ambrosio L, et al. Intervertebral disc degeneration: a focus on obesity and type 2 diabetes. *Diabetes Metab Res Rev*. 2019;36:e3224.
- Nasto LA, Ngo K, Leme AS, et al. Investigating the role of DNA damage in tobacco smoking-induced spine degeneration. *Spine J*. 2014; 14:416-423.
- Hartvigsen J, Hancock MJ, Kongsted A, et al. What low back pain is and why we need to pay attention. *Lancet*. 2018;391:2356-2367.
- Vadalà G, Ambrosio L, Russo F, Papalia R, Denaro V. Interaction between mesenchymal stem cells and intervertebral disc microenvironment: from cell therapy to tissue engineering. *Stem Cells Int*. 2019; 2019:2376172.
- Vadalà G, Russo F, Ambrosio L, et al. Biotechnologies and biomaterials in spine surgery. *J Biol Regul Homeost Agents*. 2015;29:137-147.
- Clouet J, Fusellier M, Camus A, le Visage C, Guicheux J. Intervertebral disc regeneration: from cell therapy to the development of novel bioinspired endogenous repair strategies. *Adv Drug Deliv Rev*. 2018; 146:306-324.
- Schol J, Sakai D. Comprehensive narrative review on the analysis of outcomes from cell transplantation clinical trials for discogenic low back pain. *North American Spine Society Journal (NASSJ)*. 2023;13: 100195.
- Vadalà G, Russo F, Musumeci M, et al. Clinically relevant hydrogel-based on hyaluronic acid and platelet rich plasma as a carrier for mesenchymal stem cells: rheological and biological characterization. *J Orthop Res*. 2017;35:2109-2116.
- Vadalà G, Ambrosio L, Russo F, Papalia R, Denaro V. Stem cells and intervertebral disc regeneration overview-what they can and can't do. *Int J Spine Surg*. 2021;15:40-53.
- Loibl M, Wuertz-Kozak K, Vadalà G, Lang S, Fairbank J, Urban JP. Controversies in regenerative medicine: should intervertebral disc degeneration be treated with mesenchymal stem cells? *JOR Spine*. 2019;2:e1043.
- Mathieu M, Martin-Jaular L, Lavie G, Théry C. Specificities of secretion and uptake of exosomes and other extracellular vesicles for cell-to-cell communication. *Nat Cell Biol*. 2019;21:9-17.
- Lo Cicero A, Stahl PD, Raposo G. Extracellular vesicles shuffling inter-cellular messages: for good or for bad. *Curr Opin Cell Biol*. 2015;35: 69-77.
- Buschmann D, Mussack V, Byrd JB. Separation, characterization, and standardization of extracellular vesicles for drug delivery applications. *Adv Drug Deliv Rev*. 2021;174:348-368.
- Lu L, Xu A, Gao F, et al. Mesenchymal stem cell-derived exosomes as a novel strategy for the treatment of intervertebral disc degeneration. *Front Cell Dev Biol*. 2022;9:770510.
- Liau LL, Ruzsyzmah BHI, Ng MH, Law JX. Characteristics and clinical applications of Wharton's jelly-derived mesenchymal stromal cells. *Curr Res Transl Med*. 2020;68:5-16.
- Main BJ, Maffulli N, Valk JA, et al. Umbilical cord-derived Wharton's jelly for regenerative medicine applications: a systematic review. *Pharmaceuticals*. 2021;14(11):1090.
- Williams RJ, Tryfonidou MA, Snuggs JW, le Maitre CL. Cell sources proposed for nucleus pulposus regeneration. *JOR Spine*. 2021;4: e1175.
- Abbaszadeh H, Ghorbani F, Derakhshani M, et al. Regenerative potential of Wharton's jelly-derived mesenchymal stem cells: a new horizon of stem cell therapy. *J Cell Physiol*. 2020;235:9230-9240.
- Chen P, Tang S, Gao H, et al. Wharton's jelly mesenchymal stem cell-derived small extracellular vesicles as natural nanoparticles to attenuate cartilage injury via microRNA regulation. *Int J Pharm*. 2022;623: 121952.
- Sakai D, Schol J, Bach FC, et al. Successful fishing for nucleus pulposus progenitor cells of the intervertebral disc across species. *JOR Spine*. 2018;1:e1018.
- Tilotta V, Vadalà G, Ambrosio L, et al. Mesenchymal stem cell-derived secretome enhances nucleus pulposus cell metabolism and modulates extracellular matrix gene expression in vitro. *Front Bioeng Biotechnol*. 2023;11:1152207.
- Vadalà G, Di Giacomo G, Ambrosio L, et al. *The Effect of Irisin on Human Nucleus Pulposus Cells: New Insights into the Biological Crosstalk between the Muscle and Intervertebral Disc*. Spine Publish Ahead of Print; 2022.
- Shelke GV, Lässer C, Gho YS, Lötval J. Importance of exosome depletion protocols to eliminate functional and RNA-containing extracellular vesicles from fetal bovine serum. *J Extracellular Vesicles*. 2014;3: 24783.
- Schneider CA, Rasband WS, Eliceiri KW. NIH image to ImageJ: 25 years of image analysis. *Nat Methods*. 2012;9:671-675.
- Vadalà G, Sowa GA, Kang JD. Gene therapy for disc degeneration. *Expert Opin Biol Ther*. 2007;7:185-196.
- Shalash W, Ahrens SR, Bardanova LA, Byvaltsev VA, Giers MB. Patient-specific apparent diffusion maps used to model nutrient availability in degenerated intervertebral discs. *JOR Spine*. 2021;49(4): e1179.
- Harrell CR, Fellabaum C, Jovicic N, Djonov V, Arsenijevic N, Volarevic V. Molecular mechanisms responsible for therapeutic potential of mesenchymal stem cell-derived secretome. *Cells*. 2019; 8:8.
- Russo F, Ambrosio L, Peroglio M, et al. A Hyaluronan and platelet-rich plasma hydrogel for mesenchymal stem cell delivery in the intervertebral disc: an organ culture study. *Int J Mol Sci*. 2021;22(6):2963.
- Tilotta V, Vadalà G, Ambrosio L, et al. Mesenchymal stem cell-derived exosomes: the new frontier for the treatment of intervertebral disc degeneration. *Appl Sci*. 2021;11(23):11222.
- Hingert D, Ekstrom K, Aldridge J, Crescitelli R, Brisby H. Extracellular vesicles from human mesenchymal stem cells expedite chondrogenesis in 3D human degenerative disc cell cultures. *Stem Cell Res Ther*. 2020;11:323.
- Lu K, Li HY, Yang K, et al. Exosomes as potential alternatives to stem cell therapy for intervertebral disc degeneration: in-vitro study on

- exosomes in interaction of nucleus pulposus cells and bone marrow mesenchymal stem cells. *Stem Cell Res Ther.* 2017;8:108.
34. Xia C, Zeng Z, Fang B, et al. Mesenchymal stem cell-derived exosomes ameliorate intervertebral disc degeneration via anti-oxidant and anti-inflammatory effects. *Free Radic Biol Med.* 2019;143:1-15.
  35. Liao Z, Luo R, Li G, et al. Exosomes from mesenchymal stem cells modulate endoplasmic reticulum stress to protect against nucleus pulposus cell death and ameliorate intervertebral disc degeneration in vivo. *Theranostics.* 2019;9:4084-4100.
  36. Vergroesen PP, Kingma I, Emanuel KS, et al. Mechanics and biology in intervertebral disc degeneration: a vicious circle. *Osteoarthritis Cartilage.* 2015;23:1057-1070.
  37. Cunha C, Silva AJ, Pereira P, Vaz R, Gonçalves RM, Barbosa MA. The inflammatory response in the regression of lumbar disc herniation. *Arthritis Res Ther.* 2018;20:251.
  38. Hernandez PA, Jacobsen TD, Barati Z, Chahine NO. Confocal scanning of intervertebral disc cells in 3D: inside alginate beads and in native microenvironment. *JOR Spine.* 2020;3(4):e1106.
  39. Alcaraz MJ, Compan A, Guillen MI. Extracellular vesicles from mesenchymal stem cells as novel treatments for musculoskeletal diseases. *Cell.* 2019;9(1):98.
  40. Wei W, Ao Q, Wang X, et al. Mesenchymal stem cell-derived exosomes: a promising biological tool in Nanomedicine. *Front Pharmacol.* 2020;11:590470.
  41. Cheng X, Zhang G, Zhang L, et al. Mesenchymal stem cells deliver exogenous miR-21 via exosomes to inhibit nucleus pulposus cell apoptosis and reduce intervertebral disc degeneration. *J Cell Mol Med.* 2018;22:261-276.
  42. Forsberg MH, Kink JA, Hematti P, Capitini CM. Mesenchymal stromal cells and exosomes: progress and challenges. *Front Cell Dev Biol.* 2020;8:665.

## SUPPORTING INFORMATION

Additional supporting information can be found online in the Supporting Information section at the end of this article.

**How to cite this article:** Tilotta, V., Vadalà, G., Ambrosio, L., Di Giacomo, G., Cicione, C., Russo, F., Darinskas, A., Papalia, R., & Denaro, V. (2024). Wharton's Jelly mesenchymal stromal cell-derived extracellular vesicles promote nucleus pulposus cell anabolism in an in vitro 3D alginate-bead culture model. *JOR Spine*, 7(1), e1274. <https://doi.org/10.1002/jsp2.1274>